Fluorescence Dynamics of Zinc Protoporphyrin in Solution and inside Anodized Aluminum Oxide (AAO) Nano-channel Arrays

Jin-Shyong Lin[a] (林金雄), Yu-Chying Chen[b] (陳鈺菁), Chien-Chon Chen[b] (陳建仲), Li-Yang Luo[b] (駱立揚), Eric Wei-Guang Diau[b]* (刁維光) and Tzeng-Feng Liu[a] (劉增豐)

[a]*Department of Material Science and Engineering, National Chiao Tung University, Hsinchu 30010, Taiwan, R.O.C.*

[b]*Department of Applied Chemistry and Institute of Molecular Science, National Chiao Tung University, Hsinchu 30010, Taiwan, R.O.C.*

The excited-state relaxation dynamics of zinc protoporphyrin (ZnPP) in THF solution and inside nano-channel arrays of anodized aluminum oxide (AAO) have been investigated with time-correlated single-photon-counting (TCSPC) fluorescence spectra with S_2 excitation (λ_{ex} = 435 nm). We used three initial concentrations of immersion – 4.8×10^{-6}, 4.8×10^{-5} and 4.8×10^{-4} M – to examine the extent of aggregation of ZnPP inside the AAO nano-channel arrays of two pore sizes – 15 and 70 nm. Only one decay component corresponds to the aggregation of ZnPP in THF solution, whereas at least two decay components are required to describe the transient behavior of ZnPP inside AAO. The observed systematic variation of the decay coefficients and the corresponding amplitudes of the ZnPP/AAO samples are consistent with the observation of steady-state spectra of the system reported previously (JCCS **2006**, *53*, 201), but through fluorescence lifetime measurements we further highlight the significance of aggregation of ZnPP in the specific nanoporous environment that is not achievable in ZnPP/THF solutions in large concentrations.

Keywords: AAO; Aggregation; Dye-sensitized solar cell; Porphyrin; TCSPC.

INTRODUCTION

Porphyrins have been used in the design of artificial light-harvesting systems.[1] The capacity of porphyrins to absorb visible sunlight makes these substances prospective candidates for future applications of renewable energy such as dye-sensitized solar cells and conversion of solar energy.[2-7] The UV/visible spectrum of a typical porphyrin species features an intense sharp B band at ~400 nm (S_2 state) and weak Q bands in the region 500-700 nm (S_1 state). Recent investigations[8,9] indicate that the Q-band transition can borrow intensity from the intense Soret-band transition in porphyrin aggregates. Aggregation might therefore be considered an advantageous feature for conversion of solar energy.[10-12]

We previously reported[10] a significant effect of aggregation of zinc protoporphyrin (ZnPP) inside nano-channel arrays of anodized aluminum oxide (AAO) from the observation of the variation of UV/visible absorption and fluorescent emission spectra of this system. Molecular aggregation of ZnPP molecules inside AAO nano-channel arrays is controllable according to the initial immersion concentration of the ZnPP/THF solution, the duration of immersion of the AAO substrate in the solution, and the average size of pores of AAO nano-channel arrays. Here we report the excited-state relaxation dynamics of both the ZnPP/THF solution and the ZnPP/AAO thin films using time-resolved fluorescence with ~80 ps resolution. We have observed a systematic trend for the relaxation dynamics of ZnPP inside AAO under various conditions due to formation of aggregates; the extent of aggregation is classified into four major groups according to the distribution of the fitted time coefficients.

EXPERIMENTS

Preparation of AAO Nano-channel Arrays

AAO thin-film samples with two pore diameters (d) – 15 and 70 nm – were fabricated through a one-step heating

Dedicated to the memory of the late Professor Ho Tong-Ing.

* Corresponding author. Fax: +886-3-572-3764; E-mail: diau@mail.nctu.edu.tw

treatment, described elsewhere.[10] Briefly, the AAO samples with d = 15 nm were made with 10 vol% sulfuric acid (H_2SO_4, 98%) at 8 °C, 18 V; AAO samples with d = 70 nm were made with 3 vol% oxalic acid ($C_2H_2O_4$, 99%) at 40 V, 20 °C. Since pores are randomly created on the AAO surface, a regular pattern can be obtained when AAO is removed by wet chemical etching using a mixture of 6 wt% phosphoric acid (H_3PO_4, 98%) and 1.8 wt% chromic acid (CrO_3, 95%) at 60 °C for 40 min. After the second anodization for 4 hr under the same conditions as the first anodization, the AAO nano-channel arrays would grow based on these patterns. Figs. 1A and 1B show SEM images of AAO nano-channel arrays with two pore sizes – 15 and 70 nm – respectively. The top views display a large pore density (10^9-10^{11} pores cm^{-2}), uniform pore diameter, and ordered pore arrangement of the AAO structure. The cross-sectional view (inset of Fig. 1) depicts the channels in AAO; each channel grows straight with the barrier layer at the AAO bottom.

Materials

ZnPP (Sigma-Aldrich, > 95%) was used without further purification. ZnPP was dissolved in THF (Merck, spectral grade) to form a solution with three initial concentrations – $C_i = 4.8 \times 10^{-6}$, 4.8×10^{-5} and 4.8×10^{-4} M. The AAO nanoporous substrates (disk shape, diameter 1 cm) were immersed in these ZnPP/THF solutions of constant volume (~5 mL) in a closed container near 20 °C. After immersion for 48 h, we took the ZnPP/AAO samples from the solutions and rinsed them carefully several times with pure THF to remove ZnPP molecules physically adsorbed on the surface or inside the nanotubes before the spectral and dynamics measurements.

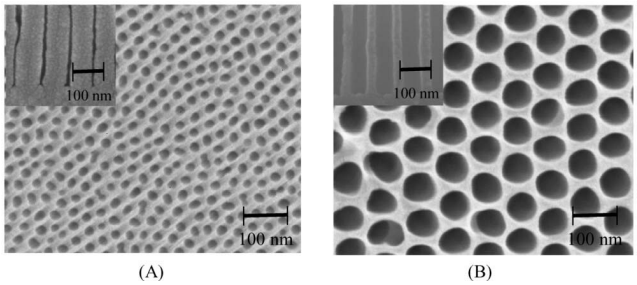

Fig. 1. SEM images of AAO made of aluminum foil (purity 99.7%): (A) top and cross-section views of AAO with pore diameter 15 nm fabricated using H_2SO_4 (10 vol%); (B) top and cross-section views of AAO with pore diameter 70 nm fabricated using $C_2H_2O_4$ solution (3 vol%).

Spectral Measurements

UV/visible reflectance/absorption spectra of ZnPP/AAO samples as thin films were measured with a composite CCD spectrometer (HR4000CG-UV-NIR, Ocean Optics) coupled with a deuterium/tungsten-halogen lamp (DH-2000, Ocean Optics) via a fiber (Y-shape, R600-UV, Ocean Optics) for reflection probes. Fluorescence spectra were obtained with another composite CCD spectrometer (USB2000FLG, Ocean Optics) with an excitation lamp containing a pulsed diode-laser head (LDH-P-C-440, PicoQuant) coupled with a laser-diode driver (PDL-800B, PicoQuant) that produces excitation pulses at 435 nm with an average power ~300 μW.

TCSPC Measurements

Fluorescence transients were recorded with a time-correlated single-photon counting (TCSPC) system (FluoTime 200, PicoQuant) with the picosecond laser source (PicoQuant) for excitation at λ_{ex} = 435 nm. The excitation pulse was focused onto the sample holder (for solution a 1-cm cuvette, but for solid films a rotating sample holder) with a lens. A lens collected emission emitted from the sample at a right angle. An iris attenuated the intensity of the detected signal; the polarization of the detected emission relative to the excitation laser pulse was set at 54.7° with a polarizer. A double monochromator of a subtractive type compensated the group-velocity dispersion of emission and selected the detection wavelength; the resolution was 8 nm with a slit of width 1 mm. A micro-channel plate photomultiplier was connected to a computer with a TCSPC-module card (SPC-630, Becker & Hickl GmbH) for data acquisition. The FWHM of the instrument response function (IRF) was typically 80 ps, measured with scattered light at the laser excitation wavelength.

RESULTS AND DISCUSSION

Emission spectra and lifetimes of ZnPP in THF solution

Fig. 2 shows emission spectra of ZnPP/THF solutions at four concentrations – $C_M = 4.8 \times 10^{-7}$, 4.8×10^{-6}, 4.8×10^{-5} and 4.8×10^{-4} M. The spectra at the former three concentrations show similar spectral features, but the relative intensities at wavelength λ_{em} = 641 nm increase gradually upon increasing concentrations when the spectra are normalized to unity at the first maximum, for which λ_{em} = 587

nm. The first emission maximum of the spectrum at the greatest concentration disappeared through the emission inner-filter effect in the region of spectral overlap between emission and absorption. Instead, a new emission maximum appeared at 608 nm, which is the result of formation of a ZnPP dimer species; higher aggregates were produced at even greater wavelengths as we have discussed previously.[10] The emission at $C_M = 4.8 \times 10^{-4}$ M was substantially quenched due to the effect of aggregation.

Fig. 3 shows emission transients of ZnPP/THF solutions at three concentrations and four typical wavelengths – λ_{em} = 590, 610, 650 and 670 nm; the excitation wavelength was fixed at λ_{ex} = 435 nm. The transients of all three solutions show a similar decay feature at λ_{em} = 590 nm (Fig. 3A), but at greater wavelengths the transients decay more rapidly at greater concentrations as clearly shown in Fig. 3D. Table 1 summarizes the transients at seven emission wavelengths in the range 580-690 nm for each concentration. The decay kinetics were successfully fitted using only one decay component, giving a single exponential decay coefficient of 2.0 ns for samples of all concentrations at λ_{em} = 580 and 590 nm. This observed 2.0-ns relaxation period is consistent with that of ZnTPP in benzene (τ = 2.0 ns)[13] due to $S_1 \rightarrow T_1$ intersystem crossing in the monomer.

The transients at all concentrations and for $\lambda_{em} > 590$ nm feature an additional decay component with a time coefficient ~0.4 ns. The relative amplitudes of the rapid decay component increase with increasing emission wavelength and concentration. This dynamical phenomenon is consistent with the spectral feature shown in Fig. 2 being due to emission spectra of ZnPP aggregates that are shifted to greater wavelengths. It has been recognized that porphyrin aggregates are formed in aqueous solutions at large porphyrin concentrations,[14] on addition of inorganic salt,[14,15] on variation of pH,[16,17] with cationic surfactants,[18] or on binding to DNA.[19] In our case, ZnPP molecules aggregate in an organic solvent, but the proportion of these aggregates is less than that of monomers even in a solution of great concentration.

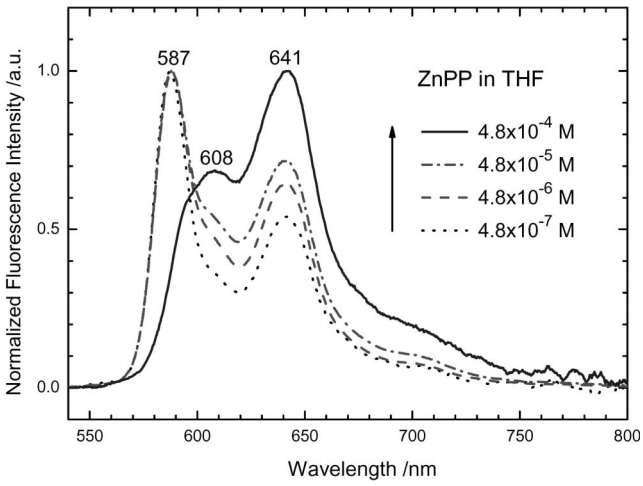

Fig. 2. Fluorescent emission spectra of ZnPP/THF solutions obtained with λ_{ex} = 435 nm at four concentrations as indicated.

Reflectance spectra of ZnPP inside AAO nano-channel arrays

The aggregation of ZnPP inside AAO nano-channel arrays is controllable through the initial concentration C_i of the ZnPP/THF solution and the pore size d of AAO nano-

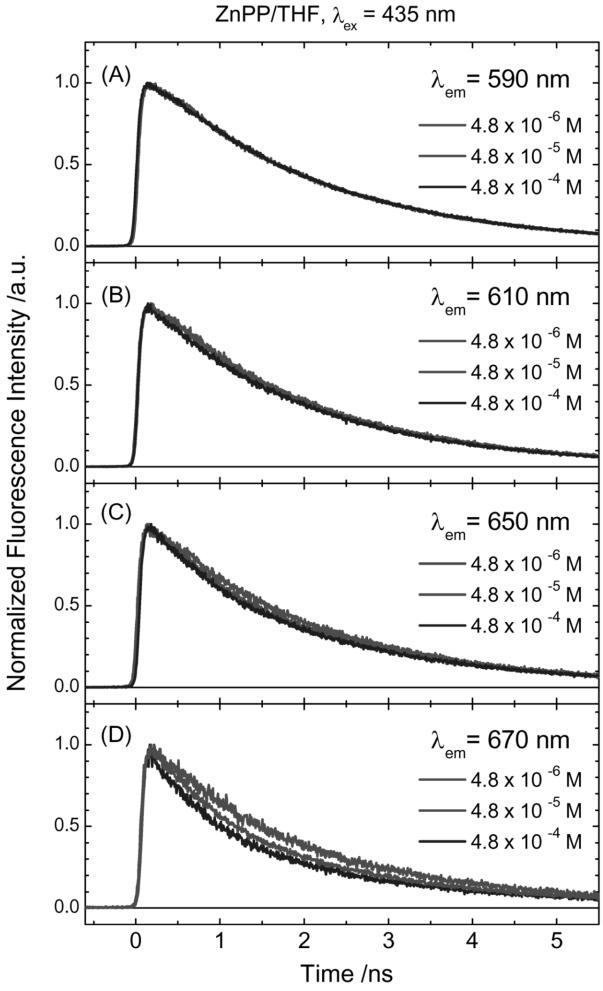

Fig. 3. Fluorescence transients of ZnPP/THF solutions obtained with λ_{ex} = 435 nm at λ_{em}/nm = (A) 590; (B) 610; (C) 650; (D) 670; fitted time parameters are listed in Table 1.

Table 1. Fitted time coefficients of fluorescence transients in ZnPP/THF solutions of various concentrations with excitation wavelength λ_{ex} = 435 nm[a]

Concentration/M	λ_{em}/nm	τ_1/ns[b]	τ_2/ns[b]
4.8×10^{-6}	580	—	2.0
	590	—	2.0
	610	0.43 (5%)	1.9 (95%)
	630	0.44 (11%)	2.1 (89%)
	650	0.43 (12%)	2.1 (88%)
	670	0.45 (24%)	2.2 (76%)
	690	0.38 (26%)	2.2 (74%)
4.8×10^{-5}	580	—	2.0
	590	—	2.0
	610	0.42 (6%)	1.9 (94%)
	630	0.42 (14%)	2.1 (86%)
	650	0.44 (22%)	2.1 (78%)
	670	0.46 (43%)	2.2 (57%)
	690	0.45 (42%)	2.2 (58%)
4.8×10^{-4}	580	—	2.0
	590	—	2.0
	610	0.30 (12%)	1.9 (88%)
	630	0.31 (20%)	2.1 (80%)
	650	0.40 (32%)	2.1 (68%)
	670	0.49 (47%)	2.2 (53%)
	690	0.45 (46%)	2.2 (54%)

[a] A parallel kinetic model is employed using the FluoFit software. [b] Relative amplitudes are shown in parentheses.

tubes. Figs. 4A-C show spectra of original reflection intensity, reflectance (R) and difference reflectance ratio (ΔR/R), respectively, for ZnPP/AAO (d = 15 nm) samples at three initial concentrations of immersion – $C_i = 4.8 \times 10^{-6}$, 4.8×10^{-5} and 4.8×10^{-4} M; the spectra of blank AAO and ZnPP/THF solution are shown for comparison. For $C_i = 4.8 \times 10^{-6}$ M, the ΔR/R pattern reflects the absorption features of the B and Q bands of ZnPP. For $C_i = 4.8 \times 10^{-5}$ M, the B band becomes broadened and the Q bands begin to grow. For $C_i = 4.8 \times 10^{-4}$ M, the maximum absorbance of the Q bands even exceeds the maximum of the B band. In contrast, the effect of aggregation becomes less significant when the average pore diameter of the AAO nano-channel arrays is enhanced (i.e., d = 70 nm), as shown in Figs. 5A-C. According to results obtained from our control experiments, we have demonstrated that the observed ΔR/R spectra of the ZnPP/AAO samples reflect the absorption features of ZnPP aggregates inside the AAO nano-structural environment – the excitonic interaction between the B and Q bands[9] systematically increases with increasing C_i or decreasing d. We have reported such a pronounced effect for ZnPP aggregates in the nano-structural environment that causes the absorption spectra of ZnPP/AAO samples to cover the entire visible spectral region.[10] Similarly, here we reanalyzed our data using the ΔR/R approach for which reflectance spectra of the system mimic the absorption spectra reported previously.[10]

Fluorescence transients of ZnPP inside AAO nano-channel arrays

We have reported that the fluorescence of ZnPP inside AAO nanoporous environments became significantly quenched because of aggregation.[10] In the present work we investigated further the effect of aggregation using the TCSPC method. The fluorescence transients of ZnPP in so-

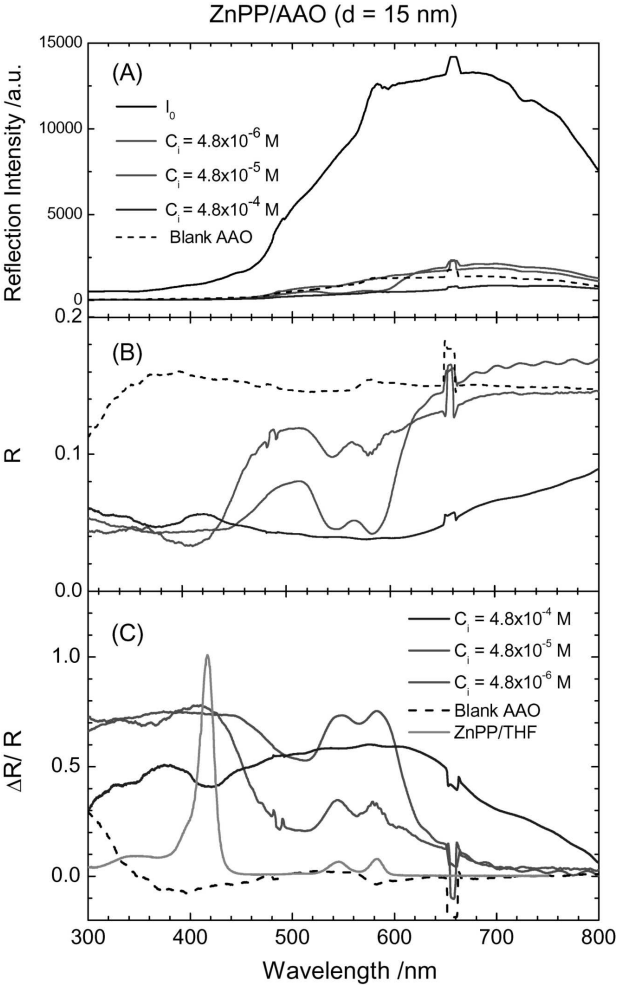

Fig. 4. (A) Reflection intensity, (B) reflection ratio, and (C) reflectance (ΔR/R) spectra of ZnPP/AAO (d = 15 nm) at three concentrations as indicated; reflectance spectrum of blank AAO and absorption spectra of ZnPP/THF solution are shown for comparison.

lution and adsorbed in AAO nano-channel arrays of pore size 15 and 70 nm are shown in Fig. 6, from A-C for $C_i = 4.8 \times 10^{-6}$, 4.8×10^{-5} and 4.8×10^{-4} M, respectively, with λ_{ex} = 435 nm and λ_{em} = 670 nm. For $C_i = 4.8 \times 10^{-6}$ M, the fluorescence decays follow a systematic trend depending on the extent of aggregation. The decay (aggregation) is more rapid (more significant) in nanotubes than in free solvents; the decay (aggregation) is also more rapid (more significant) in AAO of pore size d = 15 nm than of pore size d = 70 nm. For $C_i = 4.8 \times 10^{-5}$ and 4.8×10^{-4} M, the aggregation in AAO was so significant that the difference in transients between the samples of two pore sizes was not obviously seen, particularly for the transients obtained for $C_i = 4.8 \times 10^{-4}$ (see inset of Fig. 6C). Nevertheless, after deconvolution of the transient signals with two or three decay components and including the instrument response, perfect fits were obtained (with FluoFit software). The corresponding fitted decay coefficients for the transients of the ZnPP/AAO samples at various λ_{em} and C_i are summarized in Tables 2 and 3 for d = 15 and 70 nm, respectively.

In general, the transients were fitted with two or three decay components on varied time scales. For samples with $C_i = 4.8 \times 10^{-6}$ M and d = 15 nm, the time coefficients of the second and third components are τ_2 = 0.4-0.5 ns and τ_3 = 1.5-1.6 ns, respectively, near the lifetimes of ZnPP dimer/aggregates and monomer in solution (Table 1). The relative amplitudes are, however, disparate: the ns component is a major part of the transient in solution samples, whereas it becomes a minor part of the transient (~4%) in thin-film samples. We assign the ns components of the transients in

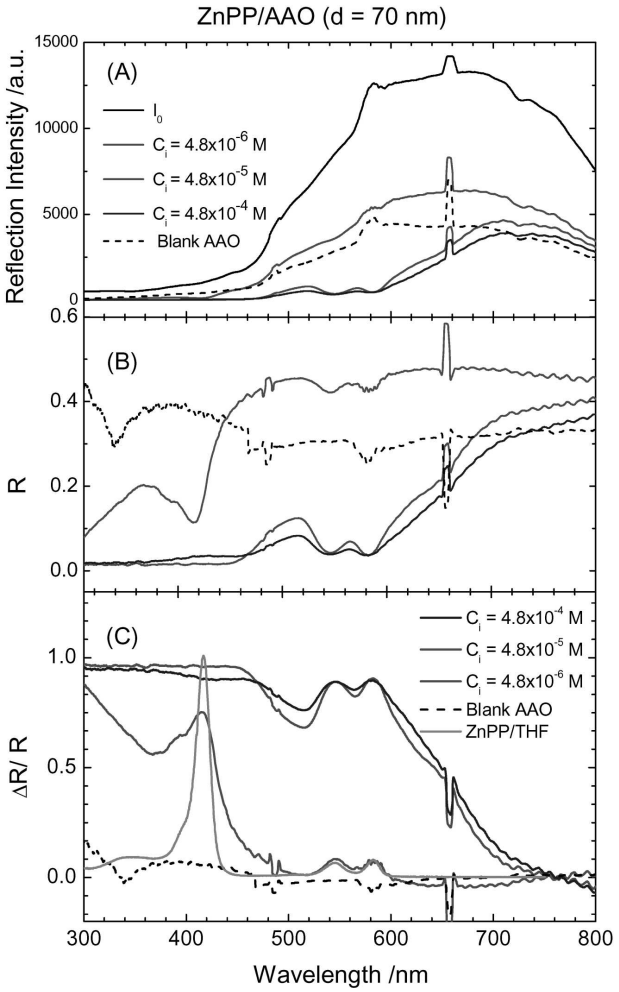

Fig. 5. (A) Reflection intensity, (B) reflection ratio, and (C) reflectance (ΔR/R) spectra of ZnPP/AAO (d = 70 nm) at three concentrations as indicated; reflectance spectrum of blank AAO and absorption spectra of ZnPP/THF solution are shown for comparison.

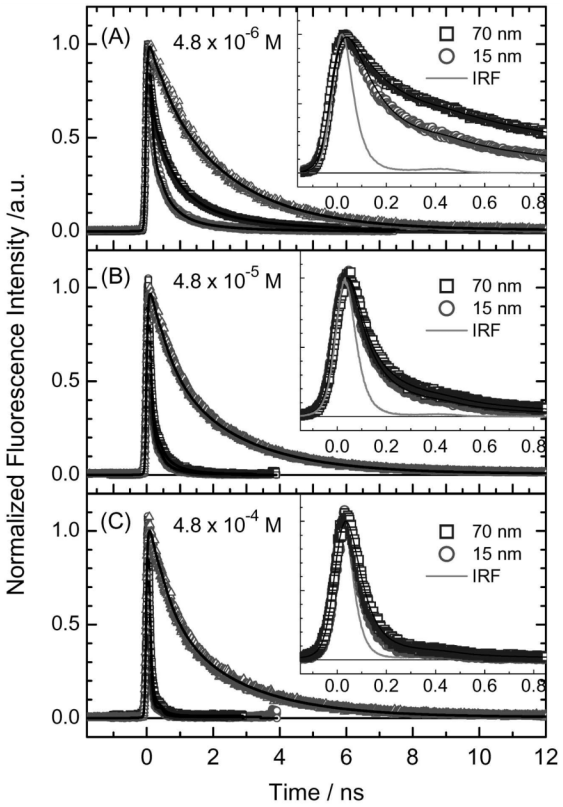

Fig. 6. Fluorescence transients of ZnPP/AAO obtained with initial immersion concentration C_i/M = (A) 4.8×10^{-6}; (B) 4.8×10^{-5}; (C) 4.8×10^{-4}. The symbols are raw data; the solid curves represent theoretical fits of the transients; fitted time parameters are listed in Table 2 (for d = 15 nm) and Table 3 (for d = 70 nm).

Table 2. Fitted time coefficients of fluorescence transients of ZnPP/AAO (d = 15 nm) thin-film samples at various initial concentrations of immersion (C_i) with excitation wavelength λ_{ex} = 435 nm[a,b]

C_i /M	λ_{em}/nm	τ_1/ps[c]	τ_2/ns[c]	τ_3/ns[c]
4.8×10^{-6}	610	69 (76%)	0.39 (19%)	1.6 (5%)
	630	70 (81%)	0.41 (16%)	1.5 (3%)
	650	82 (78%)	0.46 (18%)	1.5 (4%)
	670	83 (76%)	0.45 (20%)	1.5 (4%)
	690	91 (76%)	0.47 (20%)	1.6 (4%)
	710	92 (76%)	0.45 (20%)	1.6 (4%)
	730	96 (71%)	0.47 (25%)	1.5 (4%)
	750	97 (76%)	0.47 (20%)	1.5 (4%)
4.8×10^{-5}	610	23 (92%)	0.16 (5%)	0.56 (3%)
	630	24 (88%)	0.13 (9%)	0.56 (3%)
	650	28 (85%)	0.16 (11%)	0.58 (4%)
	670	33 (79%)	0.16 (15%)	0.57 (6%)
	690	36 (78%)	0.18 (16%)	0.58 (6%)
	710	30 (72%)	0.13 (20%)	0.50 (8%)
	730	19 (72%)	0.10 (21%)	0.50 (7%)
	750	28 (66%)	0.12 (26%)	0.50 (8%)
4.8×10^{-4}	610	20 (98%)	0.18 (2%)	—
	630	26 (97%)	0.25 (3%)	—
	650	28 (95%)	0.23 (5%)	—
	670	36 (94%)	0.26 (6%)	—
	690	33 (93%)	0.25 (7%)	—
	710	25 (95%)	0.18 (5%)	—

[a] All blank AAO samples were immersed in a ZnPP/THF solution for 48 hours.
[b] A parallel kinetic model is employed using the FluoFit software.
[c] Relative amplitudes are shown in parentheses.

samples of $C_i = 4.8 \times 10^{-6}$ M and d = 15 nm to a minor proportion of monomers inside the AAO nano-channel arrays. The values of τ_3 for nanotube samples are slightly smaller than those for free solvents because the intermolecular interactions are still involved for the former. In contrast, for samples at $C_i = 4.8 \times 10^{-6}$ M and d = 70 nm, the contribution of the third component increases to ~10% and the values of τ_3 are slightly larger than those in solution. That the values of τ_3 of the thin-film samples exceed those of the solution samples reflects the involvement of intramolecular motions for the $S_1 \rightarrow T_1$ intersystem crossing to occur. We thus observed slower relaxation dynamics for the former because the internal nuclear motions are restricted in solid films.

The first component is the major part of all transients for the ZnPP/AAO samples. The corresponding time coefficient (τ_1) was fitted in a range of 70-100 ps for samples of both d = 15 nm and 70 nm at $C_i = 4.8 \times 10^{-6}$ M, but the values of τ_1 are all in the range 20-40 ps for other transients with a greater extent of molecular aggregation. Because the FWHM of the IRF of our TCSPC system is 80 ps, we expect the time coefficients in the 20-40 ps range to be unresolved and generally described as 'IRF-limited'. The contribution of this component nevertheless reflects the extent of aggregation according to our comparison of results listed in Tables 2 and 3. For samples with $C_i = 4.8 \times 10^{-4}$ M and d = 15 nm, the aggregation was so severe that two components sufficed to fit the data; in the case of $C_i = 4.8 \times 10^{-4}$ M and d = 70 nm at greater wavelengths, a ~3% third decay component with time coefficients of 0.5-0.6 ns was required for the fit.

CONCLUDING REMARKS

We have demonstrated a significant effect of aggregation of ZnPP inside AAO nanoporous environments using picosecond time-resolved fluorescence spectroscopy.

Table 3. Fitted time coefficients of fluorescence transients of ZnPP/AAO (d = 70 nm) thin-film samples at various initial concentrations of immersion (C_i) with excitation wavelength λ_{ex} = 435 nm[a,b]

C_i /M	λ_{em}/nm	τ_1/ps[c]	τ_2/ns[c]	τ_3/ns[c]
4.8×10^{-6}	610	73 (60%)	0.64 (31%)	2.2 (9%)
	630	75 (60%)	0.63 (31%)	2.2 (9%)
	650	81 (59%)	0.64 (31%)	2.2 (10%)
	670	87 (56%)	0.64 (33%)	2.3 (11%)
	690	81 (52%)	0.57 (33%)	2.3 (15%)
	710	96 (57%)	0.59 (34%)	2.1 (9%)
	730	93 (56%)	0.59 (34%)	2.1 (10%)
	750	81 (54%)	0.52 (36%)	2.1 (10%)
4.8×10^{-5}	610	33 (83%)	0.14 (14%)	0.63 (3%)
	630	35 (77%)	0.14 (19%)	0.54 (4%)
	650	38 (70%)	0.14 (24%)	0.51 (6%)
	670	42 (61%)	0.15 (29%)	0.52 (10%)
	690	44 (59%)	0.15 (31%)	0.52 (10%)
	710	42 (60%)	0.15 (30%)	0.52 (10%)
	730	42 (35%)	0.12 (43%)	0.50 (22%)
4.8×10^{-4}	610	22 (96%)	0.17 (4%)	—
	630	21 (93%)	0.13 (7%)	—
	650	25 (83%)	0.13 (15%)	0.54 (2%)
	670	28 (82%)	0.15 (15%)	0.59 (3%)
	690	37 (83%)	0.16 (14%)	0.57(3%)
	710	36 (82%)	0.16 (15%)	0.56 (3%)
	730	21 (79%)	0.12 (18%)	0.51 (3%)

[a] All blank AAO samples were immersed in a ZnPP/THF solution for 48 hours.
[b] A parallel kinetic model is employed using the FluoFit software.
[c] Relative amplitudes are shown in parentheses.

The fitted time coefficients of the transients in the ZnPP/AAO samples are classified into four major groups. First, the 2-ns component is due to ZnPP monomers that appear only in transients at $C_i = 4.8 \times 10^{-6}$ M (for both d = 15 and 70 nm). Second, the 0.5-ns component is due to ZnPP dimers or a small extent of aggregation that appears in all transients except those at $C_i = 4.8 \times 10^{-4}$ M and d = 15 nm. Third, the 0.1 ns-component is due to a small to medium extent of aggregation that appears in all transients. Fourth, the IRF-limited component is due to a medium to large extent of aggregation that appear in all transients except those for $C_i = 4.8 \times 10^{-6}$ M. For the steady-state results, we have observed strong excitonic coupling between B and Q transitions in reflectance spectra of ZnPP aggregates formed inside AAO nano-channel arrays of varied pore size; the extent of aggregation is controllable according to the initial concentrations of immersion. Such evidence provides important information for the porphyrin/nano-channel system to be regarded as a prospective material in applications of a dye-sensitized solar cell or the conversion of solar energy.

ACKNOWLEDGEMENT

The National Science Council of the Republic of China provided financial support under contracts 95-2113-M-009-027 and 94-2120-M-009-006. Support from the MOE-ATU program is also acknowledged.

Received August 21, 2006.

REFERENCES

1. Balzani, L.; Credi, A.; Venturi, M. *Molecular Devices and Machines*; Wiley-VCH: Germany, 2003; and related references therein.
2. Kalyanasundaram, K.; Vlachopoulos, N.; Krishnan, V.; Monnier, A.; Grätzel, M. *J. Phys. Chem.* **1987**, *91*, 2342.

3. Tachibana, Y.; Haque, S. A.; Mercer, I. P.; Durrant, J. T.; Klug, D. R. *J. Phys. Chem. B* **2000**, *104*, 1198.
4. Grätzel, M. *Nature* **2001**, *414*, 338.
5. Nazeeruddin, Md. K.; Humphry-Baker, R.; Officer, D. L.; Campbell, W. M.; Burrell, A. K.; Grätzel, M. *Langmuir* **2004**, *20*, 6514.
6. Campbell, W. M.; Burrell, A. K.; Officer, D. L.; Jolley, K. W. *Coord. Chem. Rev.* **2004**, *248*, 1363.
7. Wang, Q.; Campbell, W. M.; Bonfantani, E. E.; Jolley, K. W.; Officer, D. L.; Walsh, P. J.; Gordon, K.; Humphry-Baker, R.; Nazeeruddin, M. K.; Grätzel, M. *J. Phys. Chem. B* **2005**, *109*, 15397.
8. Kano, Hideaki; Saito, T.; Kobayashi, T. *J. Phys. Chem. B* **2001**, *105*, 413.
9. Zimmermann, J.; Siggel, U.; Fuhrhop, Roder, B. *J. Phys. Chem. B* **2003**, *107*, 6019.
10. Lin, J.-S.; Chen, Y.-C.; Chen, C.-C.; Diau, E. W.-G.; Liu, T.-F. *J. Chin. Chem. Soc.* **2006**, *53*, 201.
11. Luo, L.-Y.; Lo, C.-F.; Lin, C.-Y.; Chang, I.-J.; Diau, E. W.-G. *J. Phys. Chem. B* **2006**, *110*, 410.
12. Lo, C.-F.; Luo, L.-Y.; Diau, E. W.-G.; Chang, I.-J.; Lin, C.-Y. *Chem. Comm.* **2006**, 1430.
13. Ohno, O.; Kaizu, Y.; Kobayashi, H. *J. Chem. Phys.* **1985**, *82*, 1779.
14. Shelnutt, J. A.; Dobry, M. M.; Satterlee, J. D. *J. Phys. Chem.* **1984**, *88*, 4980.
15. Kano, K.; Fukuda, K.; Wakami, H.; Nishiyabu, R.; Pasternack, R. F. *J. Am. Chem. Soc.* **2000**, *122*, 7494.
16. Inamura, I.; Uchida, K. *Bull. Chem. Soc. Jpn.* **1991**, *64*, 2005.
17. Scolaro, L. M.; Castriciano, M.; Romeo, A.; Patane, S.; Cefali, E.; Allegrini, M. *J. Phys. Chem. B* **2002**, *106*, 2453.
18. Maiti, N. C.; Mazumdar, S.; Periasamy, N. *J. Phys. Chem. B* **1998**, *102*, 1528.
19. Pasternack, R. F.; Bustamante, C.; Collings, P. J.; Giannetto, A.; Gibbs, E. J. *J. Am. Chem. Soc.* **1993**, *115*, 5393.